THE JOURNAL OF BIOLOGICAL CHEMISTRY VOL. 285, NO. 2, pp. 1229–1238, January 8, 2010

The Recognition Unit of FIBCD1 Organizes into a Noncovalently Linked Tetrameric Structure and Uses a Hydrophobic Funnel (S1) for Acetyl Group Recognition*

Received for publication, September 2, 2009 Published, JBC Papers in Press, November 5, 2009, DOI 10.1074/jbc.M109.061523

Theresa Thomsen[‡], Jesper B. Moeller[‡], Anders Schlosser[‡], Grith L. Sorensen[‡], Soren K. Moestrup[§], Nades Palaniyar[¶], Russell Wallis[‖1], Jan Mollenhauer[‡], and Uffe Holmskov[‡2]**

*From the [‡]The Medical Biotechnology Center, University of Southern Denmark, 5000 Odense, Denmark, the [§]Department of Medical Biochemistry, University of Aarhus, 8000 Aarhus, Denmark, [¶]The Hospital for Sick Children and the Department of Laboratory Medicine and Pathobiology, University of Toronto, Toronto, Ontario M5G 2M9, Canada, and the [‖]Department of Infection, Immunity and Inflammation, **Department of Biochemistry, University of Leicester, Leicester LE1 9HN, United Kingdom*

We have recently identified FIBCD1 (Fibrinogen C domain containing 1) as a type II transmembrane endocytic receptor located primarily in the intestinal brush border. The ectodomain of FIBCD1 comprises a coiled coil, a polycationic region, and a C-terminal FReD (fibrinogen-related domain) that assembles into disulfide-linked homotetramers. The FIBCD1-FReD binds Ca^{2+} dependently to acetylated structures like chitin, *N*-acetylated carbohydrates, and amino acids. FReDs are present in diverse innate immune pattern recognition proteins including the ficolins and horseshoe crab TL5A. Here, we use chemical cross-linking, combined with analytical ultracentrifugation and electron microscopy of the negatively stained recombinant FIBCD1-FReD to show that it assembles into noncovalent tetramers in the absence of the coiled coil. We use surface plasmon resonance, carbohydrate binding, and pulldown assays combined with site-directed mutagenesis to define the binding site involved in the interaction of FIBCD1 with acetylated structures. We show that mutations of central residues (A432V and H415G) in the hydrophobic funnel (S1) abolish the binding of FIBCD1 to acetylated bovine serum albumin and chitin. The double mutations (D393N/D395A) at the putative calcium-binding site reduce the ability of FIBCD1 to bind ligands. We conclude that the FReDs of FIBCD1 forms noncovalent tetramers and that the acetyl-binding site of FReDs of FIBCD1 is homologous to that of tachylectin 5A and M-ficolin but not to the FReD of L-ficolin. We suggest that the spatial organization of the FIBCD1-FReDs determine the molecular pattern recognition specificity and subsequent biological functions.

We have recently identified FIBCD1 as the first vertebrate membrane-bound chitin-binding protein (1). FIBCD1 is a type II transmembrane receptor composed of a cytoplasmic tail with two potential phosphorylation sites, a transmembrane helix, and an ectodomain. The ectodomain contains a coiled-coil region and a polycationic region with a cluster of arginines followed by a C-terminal domain homologous to the fibrinogen β- and γ-domains, referred to as the FReD (fibrinogen-related domain). FIBCD1 is expressed apically on enterocytes in the small and large intestine, and functional analyses in human cells have shown that FIBCD1 mediates endocytosis of its ligands. Furthermore, the FIBCD1-FReD binds selectively and calcium-dependently to acetylated structures including chitin, some *N*-acetylated carbohydrates and amino acids, but not to their nonacetylated counterparts, confirming that the acetyl group binding properties of FIBCD1 lies within the FReD (1). Chitin, the most abundant biopolymer next to cellulose, is a linear homopolymer of β-1,4-linked *N*-acetyl glucosamines (GlcNAc), which is commonly found in organisms such as fungi, insects, and crustaceans but not in mammals. Mammals are exposed to chitin through ingestion of or infection with organisms containing chitin. Chitin has recently been reported to serve as a molecular pattern involved in recruitment and activation of innate immune cells and in induction of cytokine and chemokine production (2, 3), and this response may modulate the allergic reaction (2, 4).

Like chitin, peptidoglycan consists of repeating acetylated carbohydrates and the soluble C-type lectin HIP/PAP acts as an innate immune receptor for peptidoglycan as well as for chitin (5). However, FIBCD1 has not shown binding activity for the peptidoglycans tested so far, indicating that a spatial requirement must exist for the three-dimensional organization of the molecular pattern, decisive for FIBCD1 binding.

FReDs are found in a number of proteins with diverse binding properties involved in immune regulation (6–9), modeling of extracellular matrix (10), angiogenesis (11), and coagulation (12). The structurally characterized FReDs of fibrinogen (13), angiopoetin-2 (14), and tachylectin 5A (TL5A)[3] of the horseshoe crab (15) and ficolins (16–18) show a similar overall structure consisting of three domains A, B, and P, where the P domain has evolved to serve as ligand binding site of the receptors. Calcium-dependent binding is also a common feature of the FReD molecules, with the calcium-binding site located in

* This work was partially supported by the Danish Council for Independent Research, Medical Sciences; the Novo Nordisk Foundation; the Lundbeck Foundation, Fonden for Lægevidenskabens Fremme; and Canadian Institutes of Health Research (MOP-84312; to N. P.).

[1] A Research Councils UK academic fellow.

[2] To whom correspondence should be addressed: Medical Biotechnology Center, Winsloevparken 25, 3, 5000 Odense C, Denmark. E-mail: uholmskov@health.sdu.dk.

[3] The abbreviations used are: TL5A, tachylectin 5A; ECP, extracellular part; PBS, phosphate-buffered saline; TBS, Tris-buffered saline; ELISA, enzyme-linked immunosorbent assay; WT, wild type; MALDI-TOF, matrix-assisted laser desorption/ionization time-of-flight mass spectrometry; Tw, Tween 20.

close proximity to the ligand-binding site in the P domain of these proteins.

Acetyl group specificity in ligand recognition is found in the ficolins, TL5A, and FIBCD1. TL5A is a plasma-derived lectin from the horseshoe crab *Tachypleus tridentatus* that binds and agglutinates Gram-positive and -negative bacteria in a calcium-dependent manner, representing an innate immune defense molecule of ancient origin (6). The ficolins are secreted proteins that upon binding of ligands activate the complement system and hereby initiate the host response (9, 19). L-ficolin binds various encapsulated bacteria (20), lipoteichoic acid (7), 1,3-β-D-glucan (21), and apoptotic cells (22). A binding specificity for *N*-acetylated compounds was initially observed (23–25) but is presently proposed to include both acetylated and carbohydrate targets through several binding sites located in the FReD (18). M-ficolin binds patterns of *N*-acetyl structures including GlcNAc, *N*-acetylgalactosamine, and sialic acid (8, 9). The crystal structures of TL5A and ficolins have been solved revealing oligomerization and localization of their ligand binding sites. The ligand-binding site S1 is described for all the proteins, and L-ficolin has three additional binding sites termed S2–S4. TL5A and M-ficolin bind acetylated structures through S1 (15, 17), whereas L-ficolin binds acetylated structures primarily through S3 (18).

Here, we investigate the oligomerization pattern of FIBCD1 particularly relevant to FReDs. We use chemical cross-linking, analytical ultracentrifugation, and electron microscopy to show that FIBCD1-FReDs form tetrameric units independent of the coiled-coil region. We also define the acetyl group and chitin-binding site using site-directed mutagenesis within the FReD of FIBCD1. Like TL5A and M-ficolin, FIBCD1 uses the S1 binding pocket to bind acetylated BSA and chitin. Finally, we demonstrate that FIBCD1 involves a calcium-binding site for ligand binding, which is located at the same position as described for other FReD-containing molecules.

EXPERIMENTAL PROCEDURES

Cloning and PCR Amplification of FIBCD1 Constructs—The constructs were generated by PCR using Phusion polymerase (Roche) and employing I.M.A.G.E clone ID 4811679 (GenBank™ accession number BC032953) as template. The primers used were 5′-CCCTGATCACGCCCACGCGC-3′ and 5′-CCCGAATTCTTACCGGGAGCCAGTGGC-3′ in generating the extracellular construct and 5′-CCCTGATCACGCCACTGGCTCCCGG-3′ and 5′-CCCGAATTCTTAGCGGTCCTCCCGGAC-3′ in generating the FReD construct. The constructs were cloned into a pFastBac™ 1 derivative, the pNT-Bac vector, kindly donated by Nicole M. Thielens (Institut de Biologie Structurale J.-P. Ebel, Grenoble, France) (26), using standard molecular biology techniques. The N-terminal His_6 epitope-tagged FReD construct was generated using the primers: 5′-CATCATCACCATCACCATGCCACTGGCTCCCGG-3′ and 5′-CCCGAATTCTTAGCGGTCCTCCCGGAC-3′ and cloned into the expression vector pSecTag/FRT/V5-His TOPO® TA (Invitrogen). Selected point mutations were created with the QuikChange XL site-directed mutagenesis system (Stratagene) using the plasmid containing the N-terminal His_6 epitope-tagged FReD of FIBCD1 as template. Complementary sets of oligonucleotide primers (~30 base pairs each) were constructed containing mutagenic substitutions corresponding to the following five mutations in the protein sequence: H415G, A432V, W443S, Y405S/Y431S, and D393N/D395A. The amino acids were mutated into a corresponding amino acid present in nonacetyl-binding FReDs in angiopoietin-2 or microfibrillar-associated protein 4. The PCR products were cloned into the expression vector pSecTag/FRT/V5-His TOPO® TA (Invitrogen). All the constructs were sequenced and analyzed for the presence of desired mutations and the absence of additional mutations.

Expression of Extracellular and FReD Domains of FIBCD1 in Insect Cells—Nontagged FReD and the extracellular part (ECP) of FIBCD1 were expressed in the Bac-to-Bac® baculovirus expression system (Invitrogen) according to the manufacturer's protocol. The Sf9 cell line was used for recombinant virus production and the High five™ cell line for protein expression. Infection of the High five™ cells was conducted at a multiplicity of infection of 1. Supernatants were harvested 72 h after infection.

Expression of Mutant and WT His-tagged FReD in HEK293 Cells—The Flp-In™ system (Invitrogen) was used to express the variants of the His-tagged FReDs in HEK293 cells essentially as described (1). Supernatants were harvested after 72 h of expression and analyzed by SDS-PAGE and Western blotting.

SDS-PAGE—Protein samples were reduced by heating at 100 °C for 1 min in sample buffer (200 mM Tris, 4% SDS, 10% glycerol, 8 M urea, 0.0145% bromphenol blue, pH 6.8) containing 60 mM dithiothreitol and alkylated by the addition of 1.4 M iodoacetamide. Unreduced samples were heated at 100 °C for 1 min in sample buffer containing 0.02 M iodoacetamide and alkylated with 1.4 M iodoacetamide. Proteins were separated using 4–12% polyacrylamide gradient gels in a discontinuous buffer system (Bio-Rad). Coomassie staining was performed for 1 h in SimplyBlue Safestain (Invitrogen) and destained overnight in H_2O. Silver staining was performed essentially as described by Nesterenko *et al.* (27).

Anti-FIBCD1 Antibodies—Polyclonal antibodies were produced in rabbit and chicken. The immunizations of the rabbit were performed using denatured antigen. Recombinant FIBCD1-FReD was heated to 80 °C for 10 min in 0.5% SDS/phosphate buffered saline (PBS) and cooled to room temperature. The preparation was diluted in PBS to 200 μg/ml. The rabbit was immunized five times with 200 μg of antigen with 2-week intervals. The rabbit was bled 10 days after the last injection, and the serum was kept at 4 °C. Davids Biotechnology, (Regensburg, Germany) performed the immunizations of the chicken and the purification of anti-FIBCD1 antibodies as described (1).

Western Blotting—Electrophoretically separated proteins were transferred onto polyvinylidene difluoride membranes (Immobilon P, Millipore) for Western blotting. For detection of recombinant FIBCD1, the membranes were incubated with a polyclonal rabbit anti-FIBCD1 antibody diluted 1:1,000 followed by horseradish peroxidase-coupled goat anti-rabbit IgG (Sigma-Aldrich) diluted 1:10,000 in TBS/Tw (140 mM NaCl, 10 mM Tris-HCl, 0.02% (w/v) NaN_2, 0.05% (v/v) Tween 20, pH 7.4).

The membranes were washed and developed using the enhanced chemiluminescence (ECL) standard method (Amersham Biosciences). The markers used were Mark12 (Invitrogen) and Precision Plus Protein Standards (Bio-Rad).

Purification of Nontagged ECP and FReD Domains of FIBCD1 on an N-Acetylated Immobilized Resin—5 ml of Toyopearl AF-amino-650 M resin (Tosoh Bioscience, Tokyo, Japan) were washed twice with distilled water and mixed with 4 ml of 0.2 M sodium acetate and 2 ml of acetic anhydride and then incubated on ice for 30 min. After incubation, 2 ml of acetic anhydride were added to the mixture, and the incubation continued for further 30 min at room temperature as described in Ref. 6. The resin was washed several times with distilled water and 1 M NaOH followed by washing with TBS, 0.5 M NaCl, 5 mM $CaCl_2$ before chromatography. Culture supernatants from High five™ cells were applied to the resin, and the resin was washed extensively with TBS, 0.5 M NaCl, 5 mM $CaCl_2$. Bound proteins were eluted in TBS, 250 mM sodium acetate. The purity of the eluted proteins was examined by SDS-PAGE and silver staining. The proteins were dialyzed against TBS and quantified using a NanoDrop ND-1000 spectrophotometer (Thermo Scientific).

Purification of Recombinant Forms of FIBCD1—Culture supernatants from HEK293 cells expressing the variant forms of FIBCD1 were dialyzed against PBS (137 mM NaCl, 3 mM KCl, 8 mM Na_2HPO_4, 1.5 mM KH_2PO_4), 0.5 M NaCl, 50 mM imidazole and applied to a HiTrap chelating HP column (GE Healthcare) on a fast protein liquid chromatography system (GE Healthcare). The column was washed extensively in PBS, 0.5 M NaCl, 50 mM imidazole, before bound proteins were eluted by applying an imidazole gradient PBS, 0–0.5 M imidazole. The purity of the eluted proteins was examined by SDS-PAGE and silver staining. The proteins were dialyzed against TBS and quantified using a NanoDrop ND-1000 spectrophotometer (Thermo Scientific).

Cross-linking Analysis—The extent of oligomerization of recombinant FIBCD1-FReD was analyzed by chemical cross-linking using glutaraldehyde. Glutaraldehyde was added to recombinant FIBCD1-FReD in molar excess from 10 to 5,000. The reactions were incubated at room temperature for 1 h, terminated by addition of SDS-PAGE sample buffer, and boiled for 2 min prior to SDS-PAGE analysis and Coomassie staining.

ELISA—Microtiter plates (Maxisorp, NUNC) were coated with 1 μg/ml of acetylated BSA (Sigma) or BSA (Sigma) and blocked with TBS/Tw before incubation with the recombinant variants of FIBCD1. The recombinant forms were added in TBS/Tw, 5 mM $CaCl_2$ in 2-fold dilutions. After incubation overnight at 4 °C and washing, the wells were incubated for 2 h at room temperature with chicken anti-FIBCD1 antibodies diluted 1:1,000 in TBS/Tw, 5 mM $CaCl_2$. The plates were washed with TBS/Tw, 5 mM $CaCl_2$ and incubated for 1 h with alkaline phosphatase-labeled anti-chicken IgY (Sigma-Aldrich) diluted 1:2,000 in TBS/Tw, 5 mM $CaCl_2$ followed by washing and development using 1 mg/ml *p*-nitrophenylphosphate, disodium salt (Boehringer) in alkaline phosphatase substrate buffer (100 mM Tris-base, 5 mM MgCl, 100 mM NaCl, pH 9.5).

Analysis of Binding of FIBCD1 to Acetylated Structures—The recombinant WT, H415G, A432V, W443S, Y405S/Y431S, and D393N/D395A forms were added from 1 μg/ml in TBS/Tw, 5 mM $CaCl_2$ in 2-fold dilutions using the ELISA-based assay against acetylated BSA as described. The binding between the WT and D393N/D395A and acetylated BSA was also tested in the presence of 10 mM EDTA or 5 mM $MnCl_2$ instead of $CaCl_2$. The signal from binding of protein to BSA was subtracted from the signal from binding to acetylated BSA. The normalized signals were expressed as a percentage of the signal from WT at 1 μg/ml (100%). The analyses were performed in triplicates, and the experiment was repeated three times. The specificity of the binding to acetylated BSA was assayed by inhibition with acetylated and nonacetylated compounds including *N*-acetyl-D-glucosamine, D-glucosamine, methyl-D-glucose, *N*-acetyl-D-galactosamine, D-galactosamine, methyl-D-galactosamine, *N*-acetyl-D-mannosamine, D-mannosamine, methyl-D-mannosamine, sodium acetate, acetylcholine, acetyl alanine, alanine, sodium butyrate, and sodium propionate. 2-Fold dilutions of inhibitor ranging from 50 to 0 mM were mixed with the nontagged FIBCD1-ECPs or FIBCD1-FReDs (62.5 ng/ml, final concentration) in TBS/Tw, 5 mM $CaCl_2$, pH 7.4. The plates were incubated at 4 °C overnight, washed, and developed as described previously. The binding to acetylated BSA was also analyzed by surface plasmon resonance analysis on a BIAcore 3000 instrument (GE Healthcare) essentially as described in Ref. 28. Briefly, acetylated BSA immobilized on a CM5 sensor chip (34 fmol receptor/mm^2) was incubated with the recombinant WT, H415G, A432V, W443S, Y405S/Y431S, and D393N/D395A forms at 250, 150, 75, and 25 nM in 10 mM HEPES, 150 mM NaCl, 3 mM $CaCl_2$, 1 mM EGTA, 0.005% surfactant P20, pH 7.4. The relative increase in response between acetylated BSA and control flow channels was determined. Kinetic parameters were determined by using the BIA evaluation 4.1 software (GE Healthcare).

Chitin-binding Assay—Chitin from crab shells (Sigma) was washed three times in TBS/Tw, 5 mM $CaCl_2$ and pelleted by centrifugation. 2 ml of supernatant from HEK293 cells expressing the recombinant WT, H415G, A432V, W443S, Y405S/Y431S, and D393N/D395A forms were added to 0.4 mg of chitin. After overnight incubation at 4 °C, the chitin pellets were washed three times in TBS/Tw, 5 mM $CaCl_2$. Bound protein was eluted from chitin by boiling samples in sample buffer and subsequently analyzed by SDS-PAGE and Western blot. To ensure that equal amount of protein was used in the chitin-binding assay, the concentration of the recombinant proteins in the supernatant were standardized by semiquantitative analysis. Films were scanned into .tif format using an HP Scanjet Pro flatbed scanner, and images were analyzed and quantitated in Adobe Photoshop following a previously described method.

Electron Microscopy of Recombinant FReD—Purified FIBCD1-FReD preparations (10 μl, 25–50 μg/ml) were incubated onto Cu^{2+} grids (200 or 400 mesh; Gilder, Marivac) supporting a plastic film coated with a thin (5–10 nm) layer of evaporated carbon. After allowing 1–2 min for sample adhesion, excess liquid was removed by blotting with torn filter papers (Whatman Reeve Angel-A). The specimen grid was then placed on a drop of 4% (w/v) uranyl acetate (J.B. EM Services, Montreal, Canada) for 30 s. The grids were then transferred to another drop of stain and allowed to stand for an additional 30 s.

Excess stain was removed with torn filter papers leaving a thin layer of stain on the grids. The stained grids were air dried for at least 1 h before examination in transmission electron microscopy. Specimens were examined at 250,000× nominal magnification using a JEOL JEM-100CX transmission electron microscopy at 80 kV. Images were captured electronically at 1.977 pix/nm, and the dimensions of single particles were measured using 1,000,000× magnified images. The inner pore diameter and the outer dimensions of the particle were made on each of the randomly selected particles ($n = 100$). The highest length of each particle (straight line from one end to the other) was first recorded, and then a similar reading was made at a 90° angle on the X-Y plane. All dimensions were rounded off to the nearest 0.01 nm and presented as means ± S.D.

Analytical Ultracentrifugation—Equilibrium experiments were carried out essentially as described previously in a Beckman XLI centrifuge using epon charcoal-filled six-hole centerpieces (29). Before analysis, all proteins were dialyzed extensively against 50 mM Tris, 150 mM NaCl, pH 7.5. Samples were centrifuged at 9,000 and 12,000 rpm at 20 °C, and scans were taken every 6 h at 254 and 280 nm until no change was detected in the protein distributions in consecutive scans, indicating that equilibrium was reached. The shape-independent molecular mass of FIBCD1-FReD was determined by fitting the equilibrium distributions from three different protein concentrations simultaneously to a single species model using the software supplied with the centrifuge. Sedimentation velocity experiments were carried out at 40,000 rpm and at 20 °C using aluminum centerpieces. Scans were collected at 2–4 min intervals at 230 nm. Data were analyzed using the program Sedfit (30). Values are displayed as by correcting for the effects of buffers (31). The partial specific volume of FIBCD1-FReD was calculated as 0.707 ml/g based on its amino acid and carbohydrate compositions (31). The molecular mass of the FIBCD1-FReD was determined independently from the $s_{20,w}$ and the Stoke's radius, derived from gel filtration experiments as described (32).

Matrix-assisted Laser Desorption/Ionization Time-of-flight Mass Spectrometry (MALDI-TOF)—Protein (6 μM in water) was mixed in a 1:1 ratio with a 10 mg/ml solution of sinapinic acid (Sigma) in 0.1% trifluoroacetic acid, 50% acetonitrile. A 0.5-μl aliquot was spotted onto a stainless steel MALDI target plate, and mass spectra were obtained using a Voyager DE-STR MALDI-TOF mass spectrometer (Applied Biosystems) in positive ion linear mode over the mass range 5,000–45,000 Da. Calibration was performed using the singly charged, doubly charged, and dimer masses of horse heart myoglobin (Sigma).

Gel Permeation Chromatography—The gel permeation chromatography was performed using a Superose™ 12 10/300 GL column (GE Healthcare) mounted onto ÄKTA fast protein liquid chromatography (GE Healthcare). The Superose™ 12 column was equilibrated using 3 bed volumes of TBS, 10 mM EDTA, and 200 μl of purified FIBCD1-ECP or FIBCD1-FReD was loaded onto the Superose™ 12 column. The fractions were diluted 3-fold in TBS/Tw, 30 mM $CaCl_2$, and the content of the elution profile was verified in an ELISA-based set up against acetylated BSA as described previously.

Molecular Modeling of FIBCD1—Molecular modeling of FIBCD1 was performed using the fully automated protein structure homology modeling server SWISS-MODEL 8.05 (33–37). The structure of TL5A (Protein Data Bank code 1JC9) was used as a template to model the FReD of FIBCD1. An initial model was made based on sequence alignment of TL5A and FIBCD1 (amino acids 240–461), which was further adjusted to match the structural properties of FIBCD1 and TL5A. A homology model of the FReD globular head was build by the server, and the figures were prepared using the MacPyMOL software (DeLano Scientific).

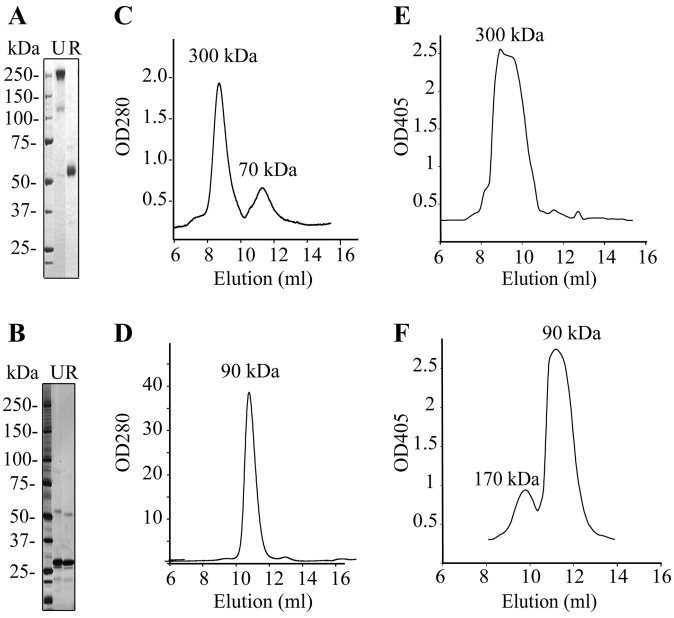

FIGURE 1. **Characterization of recombinant ECP and FReD forms of FIBCD1.** Recombinant ECP and FReD of FIBCD1 were expressed in an insect expression system and were affinity-purified on an acetylated Toyopearl AF-amino-650 M resin column. The proteins were further analyzed by gel filtration to assess oligomerization of the variant forms. SDS-PAGE analysis of unreduced (*U*) and reduced (*R*) samples of affinity-purified FIBCD1-ECPs (*A*) and FIBCD1-FReDs (*B*). Elution profiles of gel permeation chromatography of FIBCD1-ECPs (*C*) and FIBCD1-FReDs (*D*). ELISA analysis of eluted fractions of FIBCD1-ECPs (*E*) and FIBCD1-FReDs (*F*), to test for the presence of low abundance oligomers. The species at 165 kDa in *F* (probably an octamer of subunits) represented <2% of the total protein based on the data in *D* and velocity analytical ultracentrifugation data.

RESULTS

Expression of Recombinant FIBCD1 Variants and Comparison of Their Oligomerization Properties—We expressed two recombinant forms of FIBCD1 in insect cells to study the oligomerization and the binding specificity of both variants. The first recombinant form contained the entire ectodomain of FIBCD1 (FIBCD1-ECP) and the second recombinant form only included the FReD (FIBCD1-FReD). Both forms were purified by *N*-acetyl affinity chromatography using acetylated Toyopearls as a matrix. When analyzed on SDS-PAGE, the recombinant FIBCD1-ECPs migrated equivalent to a tetrameric form (~250 kDa) in the unreduced state and as a monomeric form (~60 kDa) in the reduced state (Fig. 1*A*). As expected, the recombinant FIBCD1-FReDs migrated as monomers both in the reduced and the unreduced state (~30 kDa) (Fig. 1*B*). The migration patterns suggest that the FIBCD1-ECPs form disulfide-linked tetramers in the quaternary structure, whereas no interdomain covalent linkage is found between the FIBCD1-FReDs.

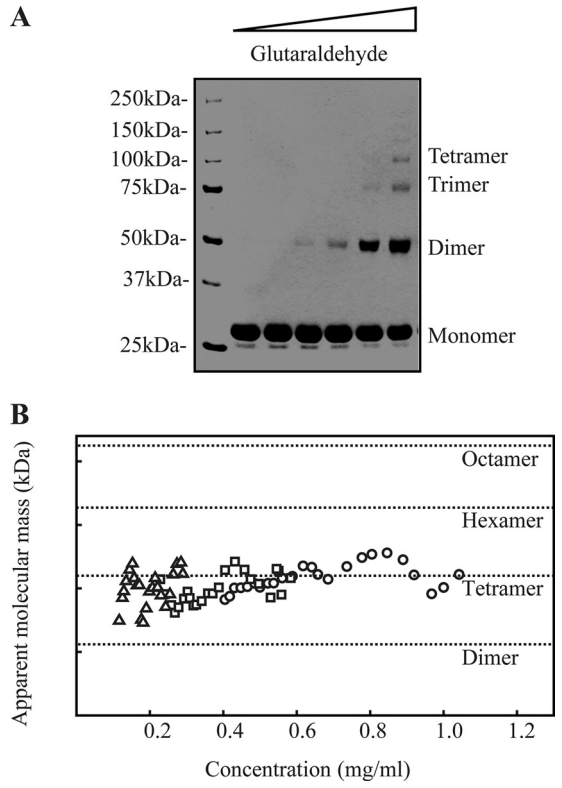

FIGURE 2. **Oligomerization of recombinant FIBCD1-FReD.** *A*, affinity-purified recombinant FReD was cross-linked with increasing concentrations of glutaraldehyde. Proteins were analyzed by SDS-PAGE in the reduced state. *B*, equilibrium sedimentation ultracentrifugation of FIBCD1. Apparent weight-averaged molecular mass distribution as a function of concentration for three loading concentrations of FIBCD1, at 9,000 rpm. The calculated masses of dimers, tetramers, hexamers, and octamers of polypeptides, based on the amino acid and carbohydrate compositions are indicated by *dotted lines*. The loading concentrations were ~0.6 mg/ml (○), 0.4 mg/ml (□), and 0.2 mg/ml (△).

FIBCD1-FReDs Assemble into Tetrameric Structures—The recombinant FIBCD1-ECPs and FIBCD1-FReDs were subjected to gel permeation chromatography. The FIBCD1-ECPs were eluted corresponding to a relative molecular mass of ~300 kDa with a smaller peak around ~70 kDa (Fig. 1*C*). The identity of the fractions corresponding to the peak at ~300 kDa was confirmed by a FIBCD1-specific ELISA, whereas no significant signal was observed in fractions corresponding to the ~70 kDa peak (Fig. 1*E*). The FIBCD1-FReDs were detected mainly as a single peak at ~90 kDa after gel permeation chromatography. This was considerably higher than the expected 30 kDa for a single FReD, suggesting that the FReDs spontaneously form higher noncovalently linked oligomers (Fig. 1*D*). A signal around ~170 kDa was detected in the FIBCD1-specific ELISA probably originating from trace amounts of a higher oligomeric form.

Chemical cross-linking of recombinant FIBCD1-FReDs showed formation of dimers, trimers, and tetramers at increasing amounts of glutaraldehyde when analyzed by SDS-PAGE (Fig. 2*A*). Octamers were also detected in small amounts at higher concentrations of glutaraldehyde (data not shown).

The MALDI-MS profile of recombinant FIBCD1-FReD was consistent with a species with an average mass of 27.3 kDa. The peak was broad (with a spread of approximately ± 0.8 kDa), and the mass value was significantly greater than the calculated mass (25.9 kDa) based on the amino acid sequence, probably reflecting glycosylation of the polypeptide during biosynthesis.

Analytical ultracentrifugation was used to determine the shape-independent molecular mass of FIBCD1-FReDs. The weight-averaged molecular mass was estimated to be 115.5 ± 2.5 kDa from two independent experiments, which corresponds closely to the mass of a tetramer of the modified polypeptide (~110 kDa). No additional self-association was detected at protein concentrations up to 1 mg/ml. A similar mass value was determined in the presence of calcium (120 ± 5 kDa), indicating that tetramerization is calcium-independent. The FIBCD1-FReDs were also analyzed by sedimentation velocity experiments and the $s_{20,w}$ was 6.9 ± 0.3 S, from two separate experiments, in agreement with a compact globular molecule. The molecular mass of the FIBCD1-FReDs was calculated from the Stoke's radius, which was determined by gel permeation chromatography, and the sedimentation coefficient. The resulting value of 100 ± 10 kDa is very similar to that determined independently by equilibrium ultracentrifugation and confirms that FIBCD1-FReDs form tetramers in solution (Fig. 2*B*).

Electron microscopy of negatively stained FIBCD1-FReDs provided high resolution images of the oligomeric structures. The images were uniform with units containing four discrete domains forming a 4-cloverleaf structure with a hole at the center (Fig. 3*A*) confirming that FIBCD1-FReD exists as tetrameric units in solution. The overall size of the molecule is 5.87 ± 0.91 nm, and the hole at the center is 1.85 ± 0.47 nm (Fig. 3*B*). Taken together, these results show that the FIBCD1-FReDs oligomerize into tetramers by noncovalent interactions independent of the coiled-coil region.

FIBCD1-FReDs Are Sufficient for Ligand Interactions in Vitro—We have previously shown that FIBCD1-ECPs bind acetylated structures (1). To test whether the FIBCD1-FReDs are sufficient for ligand interactions, we compared the binding of FIBCD1-ECPs and FIBCD1-FReDs to acetylated BSA in competition assays with various acetylated and nonacetylated carbohydrates, and the concentrations of the substances that resulted in a 50% inhibition (IC_{50}) of acetylated BSA binding were calculated. The IC_{50} values using the FIBCD1-ECP and the FIBCD1-FReDs were identical (Table 1). This suggests that the ligand-binding sites locate to the FReDs and that the tetrameric FReDs are sufficient for ligand interactions *in vitro*.

Identification of Acetyl Group and Chitin-binding Site in FIBCD1—We used a site-directed mutagenesis strategy based on sequence alignments and molecular modeling comparing the FIBCD1-FReD with the FReDs of ficolins and TL5A to determine the amino acids critical for the interaction with acetylated BSA and chitin. The crystal structure of TL5A (15) and M-ficolin (17) showed that these proteins utilize the S1 site for acetyl group specific ligand-binding. The S1 site in L-ficolin is not involved in acetyl group ligand interaction, as most of the acetylated ligands tested bound through the S3 site (18). H-ficolin does not bind acetylated structures, but binds D-fucose in the S1 site (18). Based on sequence comparisons we selected five amino acids at or in close proximity to the site S1 (Fig. 4). In addition to the wild type sequence, we introduced mutations

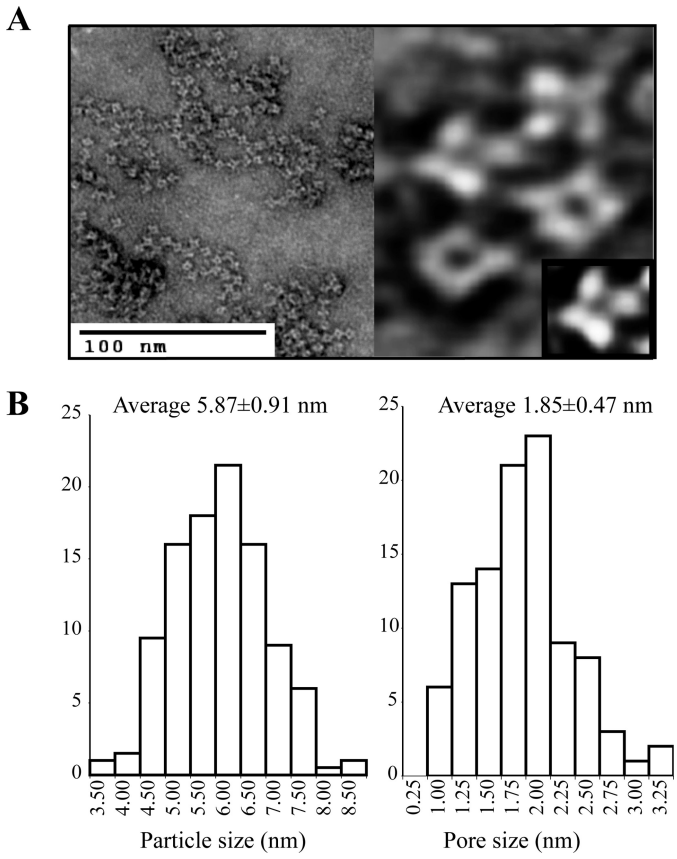

FIGURE 3. **Electron microscopy and size distributions of recombinant FIBCD1-FReD.** *A*, electron micrographs of negatively stained recombinant FReD of FIBCD1 using a JEOL JEM-100CX transmission electron microscopy electron microscope at 250,000× magnification. *B*, overall dimension and pore sizes measured using 1,000,000× magnified images from 100 randomly selected particles.

TABLE 1

The half-maximal inhibitory concentration (IC_{50}) of FIBCD1-FReD and FIBCD1-ECP binding to acetylated BSA

Inhibitor	FIBCD1-FReD	FIBCD1-ECP	I_{50} relative[a]
	mM	mM	
N-Acetyl-D-glucosamine	3.0	2.8	0.5
D-Glucosamine	NI[b]	NI	
Methyl-D-glucose	NI	NI	
N-Acetyl-D-galactosamine	2.8	2.9	0.5
D-Galactosamine	NI	NI	
Methyl-D-galactosamine	NI	NI	
N-Acetyl-D-mannosamine	1.6	1.6	1
D-Mannosamine	NI	NI	
Methyl-D-mannosamine	NI	NI	
Sodium acetate	3.1	3.1	0.5
Acetylcholine	6.7	6.6	0.2
Acetyl alanine	3.6	3.5	0.5
Alanine	NI	NI	
Sodium butyrate	NI	NI	
Sodium propionate	NI	NI	

[a] The relative inhibitor potential ("relative") was determined by dividing the IC_{50} of the best inhibitor with the IC_{50} of the desired compound.
[b] NI, not inhibitory (*i.e.* resulting in <50% at 100 mM).

giving rise to the variants: H415G, Y405S/Y431S, A432V, and W443S. Because the mutations in the FIBCD1-FReD might interfere with the purification by acetyl group affinity chromatography, we added an N-terminal His-tag for purification and expressed the proteins in stably transfected HEK293 cells. All of the variants were secreted normally indicating that the mutations did not compromise biosynthesis or folding of the FIBCD1-FReDs. The purified WT and mutated FIBCD1-FReDs are shown in Fig. 5*A*. The binding curve of WT was sigmoidal and identical to the binding curve previously described for the ECP, confirming that the N-terminal His-tag did not affect ligand binding (1). The binding of the mutated forms to immobilized acetylated BSA was also analyzed by ELISA, and the binding activity was compared with WT at concentrations up to 1 μg/ml of protein (Fig. 5*B*).

The binding activity to acetylated BSA is completely abolished in H415G and A432V and significantly reduced in Y405S/Y431S, supporting that the binding site is located in S1. The binding curve of W443S was similar but not identical to WT, and it only reached 80% of WT binding activity.

The binding of purified FIBCD1-ECP to acetylated BSA was found to be supported by the presence of calcium and manganese but not by magnesium, and it was inhibited by the presence of EDTA (1). To address the importance of the two conserved aspartates, which have been shown to coordinate calcium in L-, H-, and M-ficolins and in TL5A (Fig. 4*A*), we mutated Asp^{393} and Asp^{395} in FIBCD1-FReD. D393N/D395A abolished the binding to acetylated BSA both in presence of calcium, manganese, and EDTA (Fig. 5*C*), implying that these residues also form part of the calcium-binding site in FIBCD1.

We then immobilized acetylated BSA on a CM5 sensor ship and used changes in surface plasmon resonance as an additional approach to monitor binding of the WT and the mutated FIBCD1-FReD forms to acetylated BSA. The mutated forms all showed a diminished binding to acetylated BSA compared with the WT (Fig. 5*D*).

Finally, we also tested the variant forms in a pulldown assay with chitin. Fig. 6 shows the levels of the recombinant proteins in the supernatants of the stably transfected HEK293 cells. The expression levels of the proteins were not uniform, and, therefore, the amounts of wild type and FIBCD1-FReD mutants were standardized by comparing their band intensities on Western blots as described in "Experimental Procedures." Overall, the results of the chitin pulldown assay resembled the data obtained from the ELISA-based approach. Variants A432V and H415G did not bind to chitin, and W443S showed similar binding compared with the WT. No binding was observed in the Y405S/Y431S variant. The calcium site variant D393N/D395A also showed reduced binding to chitin.

DISCUSSION

In the present study, we have analyzed the oligomeric state and the acetyl group binding characteristics of recombinantly expressed FIBCD1 variants. We have previously shown, that the disulfide-linked ECPs of FIBCD1 form homo-tetramers indicating that FIBCD1 may form homo-tetramers in the plasma membrane. Here, our combined results using gel permeation chromatography, chemical cross-linking, analytical ultracentrifugation, and mass spectrometry show that recombinantly expressed FIBCD1-FReDs form uniform compact noncovalent globular tetramers in solution with a molecular mass of ~115 kDa. When visualized by electron microscopy of negatively stained particles, they demonstrated a symmetrical four-clover leaf structure compatible with the biophysical data. The formation of tetrameric recognition units contrasts with

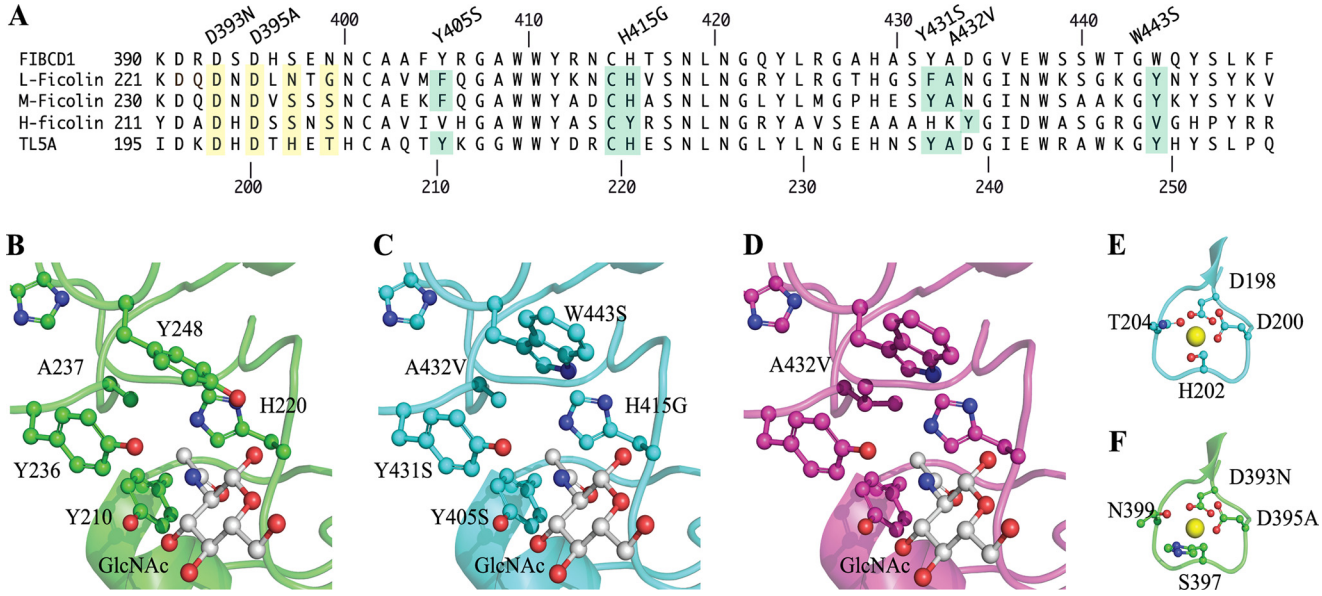

FIGURE 4. **Structure of the acetyl-binding pocket (S1) of FIBCD1.** *A*, sequence alignment of the S1 site in FIBCD1, TL5A, and the human L-, H-, and M-ficolin. Numbers on *top* and *bottom* refer to the FIBCD1 sequence and the TL5A sequence, respectively. Residues in the binding site S1 are colored *green*. Residues involved in calcium binding are colored *yellow*. The mutations performed in the study are indicated. *B*, the crystal structure of TL5A in complex with GlcNAc. *C*, modeling of the S1 binding site in FIBCD1. The mutations performed in the study are indicated. *D*, modeling of the S1 binding site in FIBCD1 containing the A432V mutation. *E*, the crystal structure of the calcium-binding site in TL5A. *F*, modeling of the calcium-binding site in FIBCD1. The mutations performed in the study are indicated. The structure of TL5A (Protein Data Bank code 1JC9) was used as a template to model the FReD of FIBCD1 by SWISS-MODEL 8.05 (33–37), and the figures were prepared using MacPyMOL software.

others multimeric FReD molecules like L-, M-, and H-ficolins (16, 18). The FReDs of these molecules form trimeric recognition units in solution and extended collagen regions stabilize the trimerization. TL5A forms disulfide linked homo-dimers that further oligomerize to hexameric and octameric bouquet-like arrangements when analyzed by electron microscopy (6). However, when TL5A was crystallized, the oligomeric arrangement was shown to be tetramers (15). In contrast to the FReDs, the carbohydrate recognition domains of C-type lectins do not self-assemble, but they need coil-coiled regions to form trimeric recognition units as exemplified by collectins like mannan-binding lectin and surfactant protein D (38, 39) or tetrameric units as in the DC-SIGN receptor (40).

In general, oligomerization of pathogen recognition receptors serves two major purposes. First, the formation of oligomeric recognition units increases binding strength compared with the monomeric form. In similarity with most lectins, the individual carbohydrate recognition domain of mannan-binding lectins display only weak affinity for sugar ligands, with dissociation constants in the millimolar range, whereas the trimeric recognition unit binds avidly to target surfaces (41, 42). The further oligomerization of the mannan-binding lectin recognition units accounts for defense mechanisms like agglutination and complement activation (43, 44).

The second purpose of forming tightly bound recognition units is to arrange an appropriate number of binding sites to match the spatial organization of highly clustered multivalent microbial molecular patterns while similar endogenous oligosaccharides are left unbound due to alternative clustering. We have previously shown that FIBCD1 binds chitin but not peptidoglycan that consists of repeating GlcNAc and *N*-acetylmuramic acid residues cross-linked by short peptides, a structure that is very similar to the $(GlcNAc)_n$ structure of chitin. Based on the present data, we speculate that this may be due to the spatial organization of the FIBCD1-FReDs.

It is well established that TL5A and L- and M-ficolin bind acetylated components (6, 8, 23, 45), but the crystal structure of the three FReDs revealed that the structural basis for this binding activity differed (15, 17, 18). The crystal structure of TL5A in complex with GlcNAc (Fig. 3*B*) (15) shows how GlcNAc is bound in a hydrophobic funnel created by the aromatic side chains of Tyr^{210} (FIBCD1, Tyr^{405}), Tyr^{236} (FIBCD1, Tyr^{431}), Tyr^{248} (FIBCD1, Trp^{443}) and His^{220} (FIBCD1, His^{415}) together with the methyl group of Ala^{237} (FIBCD1, Ala^{432}). The methyl group of GlcNAc benefits from the hydrophobic environment and lies in the middle of this funnel, and nitrogen interacts via van der Waals forces with Ala^{237} (FIBCD1, Ala^{432}) at the base of the funnel. The carbonyl oxygen atom interacts with the NH groups of His^{220} (FIBCD1, His^{415}) and the 3′-OH group interacts via a bound water molecule with the Tyr^{210} (FIBCD1, Tyr^{405}) side chain hydroxyl group (15).

The homologous binding site (designated S1-binding site) is also present in L- and M-ficolin. In M-ficolin, acetylated carbohydrates occupy the S1-binding site (17), but although L-ficolin binds acetylated compounds with high affinity, no ligands were found in the hydrophobic funnel when the crystal structure was analyzed in complex with acetylated ligands (18). Instead, L-ficolin bound the acetylated ligands primarily through the S3 site, which is structurally distinct from the S1 site. The surprising lack of acetyl group specificity in the S1 site of L-ficolin is presumably due to the replacement of a tyrosine with phenylalanine (Y262F) in L-ficolin, as the corresponding substitution in M-ficolin was found to decrease binding to GlcNAc drastically (46). On the other hand, Tyr^{210} in TL5A has been substituted with a phenylalanine in M-ficolin without having any influence on the acetyl group binding ability.

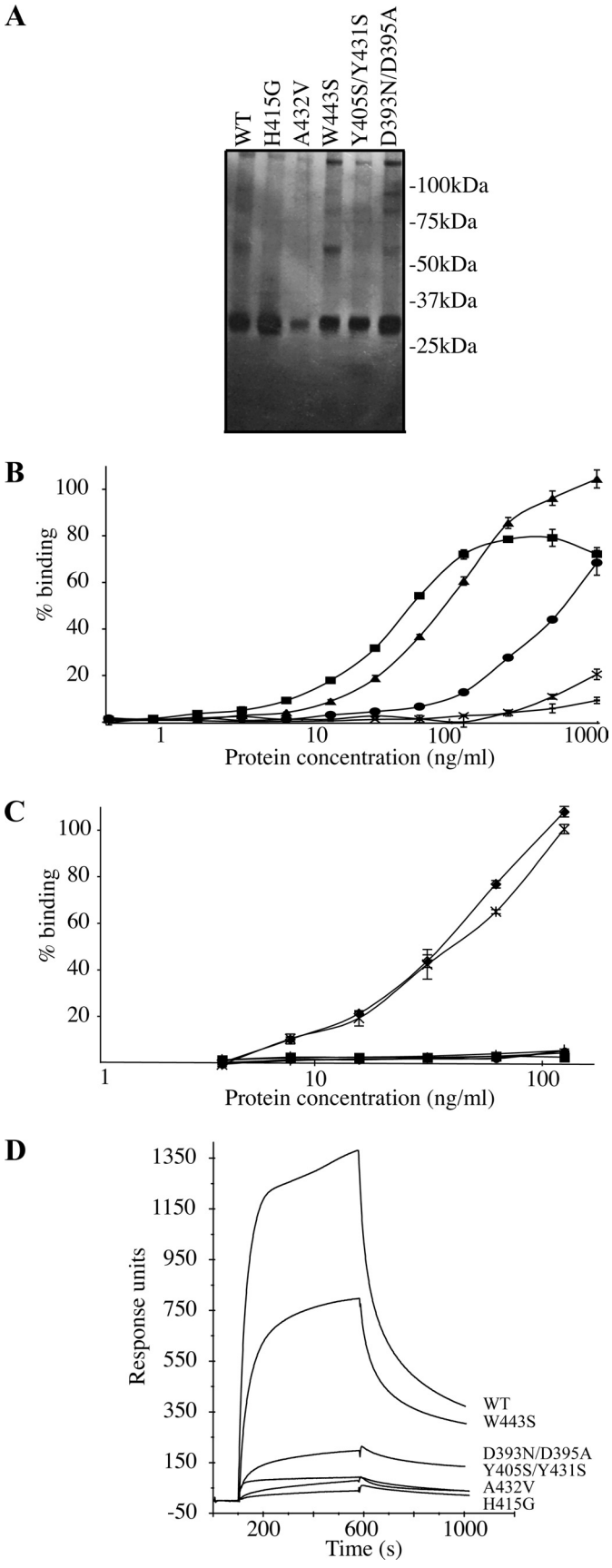

FIGURE 5. **Effects of the mutations on the ability of binding to acetylated BSA.** *A*, His-tagged forms of FIBCD1-FReDs were expressed in HEK293 cells and applied to a HiTrap chelating HP column on a fast protein liquid chromatography system and eluted with a gradient of imidazole. SDS-PAGE analysis of WT, H415G, A432V, W443S, Y405S/Y431S, and D393N/D395A. *B*, microtiter plates were coated with acetylated BSA or BSA, and the recombinant variants of His-tagged forms of FIBCD1-FReD were added from 1 μg/ml in a 2-fold dilution series in TBS/Tw containing 5 mM $CaCl_2$. The normalized signals were expressed as a percentage of the signal from WT at 1 μg/ml (100%). WT (▲), H415G (×), A432V (-), W443S (■), and Y405S/Y431S (●). *C*, microtiter plates were coated with acetylated BSA and increasing amounts of WT or D393N/D295A were added in the presence 5 mM $CaCl_2$, 5 mM $MnCl_2$ or 10 mM EDTA. The normalized signals were expressed as a percentage of the signal from WT at 125 ng/ml (100%). WT/$CaCl_2$ (♦), WT/$MnCl_2$ (×), WT/EDTA (|), D393N/D395A/$CaCl_2$ (■), D393N/D395A/$MnCl_2$ (●), and D393N/D395A/EDTA (-). *D*, surface plasmon resonance analysis of the interaction with immobilized acetylated BSA.

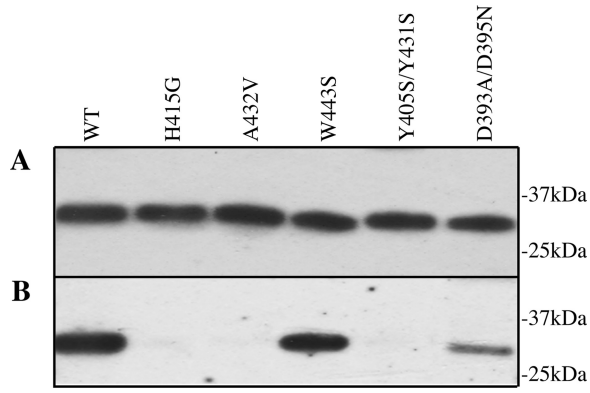

FIGURE 6. **Effects of the mutations on the ability of binding to chitin.** *A*, Western blot analysis of the recombinant mutant and WT forms of FIBCD1-FReD. Supernatants from the HEK293 cells expressing the different variants were standardized by comparing the intensities of bands to ensure equal amount of protein in the pulldown assay. The samples were analyzed by SDS-PAGE under nonreducing conditions and analyzed by Western blotting. *B*, pulldown analysis of supernatants containing the recombinant forms of the FIBCD1 and insoluble chitin. Chitin (0.5 mg) was incubated with 2 ml of standardized supernatant, and the bound protein was eluted from the insoluble chitin fraction after extensive washing. Pellet fractions were submitted to SDS-PAGE under nonreducing conditions and analyzed by Western blotting.

The residues in TL5A that form the S1 binding site are essentially conserved in FIBCD1 with the main difference being Tyr^{248} substituted by a tryptophan residue (Fig. 4*A*). We mutated several of the homologous amino acids in FIBCD1 that were found to be essential for the binding of GlcNAc in TL5A to investigate whether FIBCD1 also exploits S1 as the acetyl group-binding site (Fig. 4*C*). The binding pattern of the WT and mutated forms of the FIBCD1-FReDs were analyzed by surface plasmon resonance analysis, solid phase binding assays, and chitin pulldown assays. We found that the binding to acetylated BSA and chitin was abolished in H415G and A432V and slightly diminished in W443S compared with the WT (Figs. 5 and 6). Although the FReDs of FIBCD1 and TL5A recognize acetylated structures, Trp^{443} was not conserved between these two molecules. Therefore, our results are consistent with the fact that this amino acid is not essential for acetyl group binding. The double mutation Y405S/Y431S reduced the binding of FIBCD1 to acetylated BSA compared with the WT and showed no binding in the chitin pulldown experiment. The difference observed in the binding pattern is presumably due to a difference in the density of the acetyl groups and the influence of the remaining structure of the ligand. Chitin is composed of repeated units of GlcNAc, whereas the glucosamine is not present in acetylated BSA. Tyr^{405} and Tyr^{431} are most likely involved in maintaining the

hydrophobicity of the funnel, and this is reflected by the diminished binding to acetylated BSA. Binding toward the glucosamine unit in chitin is probably also abolished by the Y405S mutation, which, in combination with a different density of acetylation, may lead to the lack of binding to chitin.

The Ala^{432} at the base of S1 is particularly important in the binding of acetylated ligands. The replacement of alanine at the base of S1 with a valine containing two extra methyl groups probably results in minimal changes at the structural level (Fig. 4*D*). Nevertheless this mutation results in a complete loss of binding, eliminating the contacts between the ligand and other amino acids in S1. In addition, we have shown that propionate and butyrate, which compared with acetate, contain one and two extra methyl groups, respectively, cannot inhibit the binding to acetylated BSA (Table 1).

The H415G mutation also blocks the FIBCD1-FReD binding to acetylated BSA and chitin. The functionality of several histidines in the acetyl-binding area has been described in M-ficolin, including His^{284} (FIBCD1, His^{415}). A pH-dependent conformational switch in the binding of ligand was observed in M-ficolin, and a two-state conformational equilibrium model depending on the charged state of histidines in the acetyl-binding region was proposed to facilitate ligand release at low pH in acidic compartments (17). The physiological relevance of this was underlined by the recent finding of ficolin-B (the murine counterpart to M-ficolin) in lysosomes of activated macrophages (47). FIBCD1 facilitates the endocytosis of acetylated BSA (1), and the direction of acetylated components for degradation in the endosome would require ligand release, which would consecutively allow FIBCD1 to be recirculated to the membrane. We are currently investigating the importance of the other histidines for the binding to acetylated structures to determine whether these are involved in similar mechanisms as described in M-ficolin.

The crystal structures of FReDs have revealed similar coordination geometries in their calcium-binding sites, although not all ligand-FReD interactions are calcium-dependent (15, 16, 22). The binding by FIBCD1-FReD to acetylated structures is calcium-dependent (1) and, indeed, site-directed mutagenesis of the two conserved aspartates (Asp^{393} and Asp^{395}) diminishes the binding of FIBCD1 to acetylated BSA and to chitin. This locates the calcium dependence to the same site as described for TL5A, the ficolins, fibrinogen, and angiopoietin-2. The calcium-independent bindings observed in the chitin pulldown experiment and the surface plasmon resonance analysis are either because the calcium-binding is not completely blocked by the mutations or because the binding is not entirely calcium-dependent, as has been observed previously in some ficolin-ligand interactions (23).

In conclusion, the current studies reveal that the FReD subunit of FIBCD1 oligomerizes into tetrameric units by noncovalent interactions, and the acetyl-binding site is situated in S1. It appears that the acetyl group-binding domains of FIBCD1 and M-ficolin have essentially preserved the general binding characteristics of TL5A during evolution but that the spatial organization of the binding domains could define which molecular patterns containing the target groups are accepted as ligands.

REFERENCES

1. Schlosser, A., Thomsen, T., Moeller, J. B., Nielsen, O., Tornøe, I., Mollenhauer, J., Moestrup, S. K., and Holmskov, U. (2009) *J. Immunol.* **183,** 3800–3809
2. Reese, T. A., Liang, H. E., Tager, A. M., Luster, A. D., Van Rooijen, N., Voehringer, D., and Locksley, R. M. (2007) *Nature* **447,** 92–96
3. Lee, C. G., Da Silva, C. A., Lee, J. Y., Hartl, D., and Elias, J. A. (2008) *Curr. Opin Immunol.* **20,** 684–689
4. Strong, P., Clark, H., and Reid, K. (2002) *Clin. Exp. Allergy* **32,** 1794–1800
5. Cash, H. L., Whitham, C. V., Behrendt, C. L., and Hooper, L. V. (2006) *Science* **313,** 1126–1130
6. Gokudan, S., Muta, T., Tsuda, R., Koori, K., Kawahara, T., Seki, N., Mizunoe, Y., Wai, S. N., Iwanaga, S., and Kawabata, S. (1999) *Proc. Natl. Acad. Sci. U.S.A.* **96,** 10086–10091
7. Lynch, N. J., Roscher, S., Hartung, T., Morath, S., Matsushita, M., Maennel, D. N., Kuraya, M., Fujita, T., and Schwaeble, W. J. (2004) *J. Immunol.* **172,** 1198–1202
8. Frederiksen, P. D., Thiel, S., Larsen, C. B., and Jensenius, J. C. (2005) *Scand J. Immunol.* **62,** 462–473
9. Liu, Y., Endo, Y., Iwaki, D., Nakata, M., Matsushita, M., Wada, I., Inoue, K., Munakata, M., and Fujita, T. (2005) *J. Immunol.* **175,** 3150–3156
10. Chiquet-Ehrismann, R., and Tucker, R. P. (2004) *Int J Biochem. Cell Biol.* **36,** 1085–1089
11. Jones, P. F. (2003) *J. Pathol.* **201,** 515–527
12. Farrell, D. H. (2004) *Curr. Opin. Hematol.* **11,** 151–155
13. Yee, V. C., Pratt, K. P., Côté, H. C., Trong, I. L., Chung, D. W., Davie, E. W., Stenkamp, R. E., and Teller, D. C. (1997) *Structure* **5,** 125–138
14. Barton, W. A., Tzvetkova, D., and Nikolov, D. B. (2005) *Structure* **13,** 825–832
15. Kairies, N., Beisel, H. G., Fuentes-Prior, P., Tsuda, R., Muta, T., Iwanaga, S., Bode, W., Huber, R., and Kawabata, S. (2001) *Proc. Natl. Acad. Sci. U.S.A.* **98,** 13519–13524
16. Tanio, M., Kondo, S., Sugio, S., and Kohno, T. (2007) *J. Biol. Chem.* **282,** 3889–3895
17. Garlatti, V., Martin, L., Gout, E., Reiser, J. B., Fujita, T., Arlaud, G. J., Thielens, N. M., and Gaboriaud, C. (2007) *J. Biol. Chem.* **282,** 35814–35820
18. Garlatti, V., Belloy, N., Martin, L., Lacroix, M., Matsushita, M., Endo, Y., Fujita, T., Fontecilla-Camps, J. C., Arlaud, G. J., Thielens, N. M., and Gaboriaud, C. (2007) *EMBO J.* **26,** 623–633
19. Zhang, J., Koh, J., Lu, J., Thiel, S., Leong, B. S., Sethi, S., He, C. Y., Ho, B., and Ding, J. L. (2009) *PLoS Pathog* **5,** e1000282
20. Krarup, A., Sørensen, U. B., Matsushita, M., Jensenius, J. C., and Thiel, S. (2005) *Infect Immun.* **73,** 1052–1060
21. Ma, Y. G., Cho, M. Y., Zhao, M., Park, J. W., Matsushita, M., Fujita, T., and Lee, B. L. (2004) *J. Biol. Chem.* **279,** 25307–25312
22. Kuraya, M., Ming, Z., Liu, X., Matsushita, M., and Fujita, T. (2005) *Immunobiology* **209,** 689–697
23. Krarup, A., Thiel, S., Hansen, A., Fujita, T., and Jensenius, J. C. (2004) *J. Biol. Chem.* **279,** 47513–47519
24. Matsushita, M., Endo, Y., and Fujita, T. (2000) *J. Immunol.* **164,** 2281–2284
25. Matsushita, M., Endo, Y., Taira, S., Sato, Y., Fujita, T., Ichikawa, N., Nakata, M., and Mizuochi, T. (1996) *J. Biol. Chem.* **271,** 2448–2454
26. Rossi, V., Bally, I., Thielens, N. M., Esser, A. F., and Arlaud, G. J. (1998) *J. Biol. Chem.* **273,** 1232–1239
27. Nesterenko, M. V., Tilley, M., and Upton, S. J. (1994) *J Biochem. Biophys. Methods* **28,** 239–242
28. Hvidberg, V., Maniecki, M. B., Jacobsen, C., Højrup, P., Møller, H. J., and Moestrup, S. K. (2005) *Blood* **106,** 2572–2579
29. Wallis, R., and Drickamer, K. (1997) *Biochem. J.* **325**, 391–400
30. Schuck, P. (2000) *Biophys. J.* **78,** 1606–1619
31. Laue, T. M., Bhairavi, D. S., Ridgeway, T. M., and Pelletier, S. L. (1992) in *Analytical Ultracentrifugation in Biochemistry and Polymer Science* (Harding, S. E., Rowe, A. J., and Horton, J. C., eds) pp. 90–125, *Royal Society of Chemistry*, Cambridge, United Kingdom
32. Girija, U. V., Dodds, A. W., Roscher, S., Reid, K. B., and Wallis, R. (2007) *J. Immunol.* **179,** 455–462

33. Arnold, K., Bordoli, L., Kopp, J., and Schwede, T. (2006) *Bioinformatics* **22,** 195–201
34. Kopp, J., and Schwede, T. (2004) *Nucleic Acids Res.* **32**, D230–234
35. Schwede, T., Kopp, J., Guex, N., and Peitsch, M. C. (2003) *Nucleic Acids Res.* **31,** 3381–3385
36. Guex, N., and Peitsch, M. C. (1997) *Electrophoresis* **18,** 2714–2723
37. Peitsch, M. C. (1995) *Bio/Technology* **13,** 658–660
38. Weis, W. I., and Drickamer, K. (1994) *Structure* **2,** 1227–1240
39. Zhang, P., McAlinden, A., Li, S., Schumacher, T., Wang, H., Hu, S., Sandell, L., and Crouch, E. (2001) *J. Biol. Chem.* **276,** 19862–19870
40. Feinberg, H., Guo, Y., Mitchell, D. A., Drickamer, K., and Weis, W. I. (2005) *J. Biol. Chem.* **280,** 1327–1335
41. Iobst, S. T., and Drickamer, K. (1994) *J. Biol. Chem.* **269,** 15512–15519
42. Iobst, S. T., Wormald, M. R., Weis, W. I., Dwek, R. A., and Drickamer, K. (1994) *J. Biol. Chem.* **269,** 15505–15511
43. Teillet, F., Dublet, B., Andrieu, J. P., Gaboriaud, C., Arlaud, G. J., and Thielens, N. M. (2005) *J. Immunol.* **174,** 2870–2877
44. Holmskov, U., Thiel, S., and Jensenius, J. C. (2003) *Annu Rev. Immunol.* **21,** 547–578
45. Krarup, A., Mitchell, D. A., and Sim, R. B. (2008) *Immunol. Lett.* **118,** 152–156
46. Tanio, M., and Kohno, T. (2009) *Biochem. J.* **417,** 485–491
47. Runza, V. L., Hehlgans, T., Echtenacher, B., Zähringer, U., Schwaeble, W. J., and Männel, D. N. (2006) *J. Endotoxin. Res.* **12,** 120–126